Modeling tree decline trends using hybrid feature engineering and climatic trend analysis

Mohamamd Javad Soltani[1], Hooman Latifi[1*], Sajad Bahraini Moghadam[1], Marziye Ghasemi[1]

[1] Department of Photogrammetry and Remote Sensing, Faculty of Geodesy and Geomatics Engineering, K. N. Toosi University of Technology, Tehran, Iran - mamadjs@email.kntu.ac.ir, hooman.latifi @kntu.ac.ir, s.bahrainimoghadam@email.kntu.ac.ir, mrzghasemi@email.kntu.ac.ir,

KEY WORDS: Decline, Time Series, Trend Analysis, Climatical Data, Random Forest, feature selection, feature extraction.

ABSTRACT:

Forest decline poses a critical threat to the ecological function and long-term preservation of forest ecosystems. In dearth of comprehensive field measurements, remote sensing data support forest decline monitoring by offering consistent spatial and temporal observations. However, many approaches rely on costly data or lack structured feature management, limiting their applicability and performance. Freely available data like Sentinel-2 and Landsat, along with well-designed input features, enhance the efficiency and scalability of tree decline modeling. Here, we analyzed both a classified decline dataset (four discrete classes) and a continuous Phenological Decline Index (PDI) derived from Unmanned aerial vehicle (UAV) imagery, where hybrid feature selection and feature exteraction optimized inputs for the subsequent Random Forest (RF) regression and classification. The 9-year decline trend was predicted and smoothed using locally estimated scatterplot smoothing (LOESS) trend analysis, while trends of ERA5 climate data were assessed via the Sequential Mann-Kendall test. Results highlight the importance of feature selection even for non-parametric models like RF, improving R^2 from 0.40 to 0.60 and reducing RMSE from 0.13 to 0.10. Predicting PDI resulted in more consistent trends than the classification, revealing its effectiveness. Moreover, decline patterns proved highly complex and not directly aligned with climatic trends, which indicates that trees may have adapted to environmental stress. The study confirms the effectiveness of PDI methods and shows that tree decline patterns are only partially linked to climate variables.

1. INTRODUCTION

1.1 Tree decline

Tree decline is a complex ecological phenomenon characterized by progressive deterioration of tree health, often culminating in their widespread mortality. Unlike abrupt disturbances such as fires or clear-cutting, decline typically unfolds gradually, driven by multifactorial stressors that include climatic extremes, pest infestations, and anthropogenic pressures (Allen et al., 2010).
The Zagros Forests of Iran span around 6 million ha, accounting for ca. 44% of the country's forests, and are characterized by a semi-arid, semi-Mediterranean climate. Over time, this ecologically significant region has faced persistent threats such as anthropogenic disturbance, forest fires, dust storms and prevalence of pathogens (Fakhri and Latifi, 2021; Ghasemi et al., 2024b). Whereas systematic field measurements are tremendously scarse across the region, remote sensing offers cost-effective alternatives for monitoring tree decline, for example by enabling detection of canopy stress through vegetation and water indices, allowing timely subsequent conservation and restoration efforts (Pontius et al., 2020). Here, we integrate a suite of well-established but previously isolatedly applied approaches like machine leanring, feature engineering, and trend analysis to introduce a new framework for modleing tree decline trajectories in semi-arid Zagros forests of Iran.

1.2 Relevant platforms and sensors

A wide range of active/passive data including those from Landsat, MODIS, Sentinel-2, airborne LiDAR, and UAV-based hyperspectral sensors have been utilized to monitor forest decline (Torres et al., 2021). Landsat imagery provides long-term historical records that are ideal for multi-decadal trend analysis, while other openly accessible data like Sentinel-2 offer higher spatial resolutions, a prerequisite for regional to local assessments (Hirschmugl et al., 2017). While UAV- and hyperspectral/LiDAR sensors can provide more detailed information, Sentinel-2 data has gained increasing attention due to its free accessibility, combination of 10–20 m spatial resolution bands, frequent revisit time of 5 days, and broad spectral range including red-edge bands, which are particularly effective in detecting early vegetation stress (Immitzer et al., 2019); Recently, Sentinel-2 has enabled extraction of structural attributes like forest height and fractional canopy cover (Fakhri et al., 2025), which are pivotal for subsequent use in tree decline assessments.

1.3 Frequently used climatic variables

Climatic stressors such as droughts, heatwaves, and shifting rainfall patterns are amongst the potential key drivers of forest decline. Standard indices like standardized precipitation evapotranspiration index (SPEI) and Palmer drought severity index (PDSI), along with temperature anomalies and drought metrics, have been previously used to quantify stress and predict canopy dieback before visible symptoms appear (Eliades et al., 2024).
Review of the available literature shows a number of relevant cases. For example, major oak-decline trajectories in southern Portugal coincided with SPEI minima in 1994, 2005, and 2012, highlighting the index's utility in pinpointing stress thresholds (Vicente-Serrano et al., 2010). The 2018 European drought, characterized by extreme soil moisture deficits and vapor-pressure-deficit anomalies, drove unprecedented disturbance rates persisting up to two years post-drought (Senf and Seidl, 2021). Furthermore, hydraulic failure from combined heat and drought underpins widespread tree vulnerability, with global

* Corresponding Author

convergence in narrow hydraulic safety margins across biomes (Choat et al., 2012).

1.4 Decline predictor model

Modeling forest decline has recently evolved from simple statistical regressions to the integration of advanced machine learning and deep learning frameworks (Eliades et al., 2024). These models commonly integrate diverse inputs such as climatic variables, spectral indices, topographic features, and structural vegetation attributes as potential descriptors to predict susceptibility to or severity of decline (Simarmata et al., 2025). Among the plethora of approaches, conventional models like Random Forest (RF) and Gradient Boosting are favored for their robustness in classification tasks and their ability to rank feature importance (Breiman, 2001). More recently, neural network-based models like Long Short-Term Memory (LSTM) networks have been employed for analyzing time-series vegetation trends, while Convolutional Neural Networks (CNNs) are used for classification of high-resolution imagery (Kirsch et al., 2025). These architectures offer superior capacity in capturing hidden patterns and nonlinear relationships crucial in ecological processes such as decline. Despite the advanced pattern recognition capabilities of deep learning compared to machine learning models, their substantial data requirements limit their applicability in decline studies (Ghasemi et al., 2024a). The latter, which require less data and still capture complex relationships, have also been shown to outperform semi-parametric generalizted additive model (GAM) in capturing tree decline patterns due to its better resistance against overfitting, handling high-dimensional data, and providing ranked feature importances(Ghasemi et al., 2024b).

1.5 Trend analysis

Detection and analysis of trends in vegetation dynamics is fundamental to understanding their decline. Common methods include parametric approaches like linear regression and non-parametric methods such as the Mann–Kendall (MK), Sen's slope estimator, and Breaks for additive season and trend (BFAST) (Verbesselt et al., 2010). While regression captures global trends, non-parametric tests are more robust to non-normality and abrupt changes (De Jong et al., 2011).
Furthermore, the sequential MK (sMK) test extends the classical MK method by detecting both the presence and onset of monotonic trends, making it especially beneficial for early ecosystem stress detection before visible degradation (Shadmani et al., 2012). The Locally estimated scatterplot smoothing (LOESS) analysis offers a flexible, non-parametric approach to modeling complex, nonlinear patterns in time series data. By fitting simple local polynomials, LOESS adapts to local variations without imposing a global functional form, making it particularly suitable for early detection of ecosystem stress signals prior to the occurrence of visible degradation (Cleveland and Devlin, 1988).
Here, we propose a hybrid feature engineering framework that combines feature selection and extraction for both regression and classification of tree decline. By analyzing continuous and categorical decline indicators across two study areas, the approach enables evaluation of trend consistency under varying data structures. Additionally, it examines the influence of climatic stressors on decline trajectories, offering scalable, medium-resolution insights through integrating trend analysis and machine learning.

2. MATERIALS AND METHODS

2.1 Study area and reference data

This study focused on two representative sites within the central zone of Zagros forests, located in the provinces of Fars and Chaharmahal-and-Bakhtiari in Iran (Figure **1**).

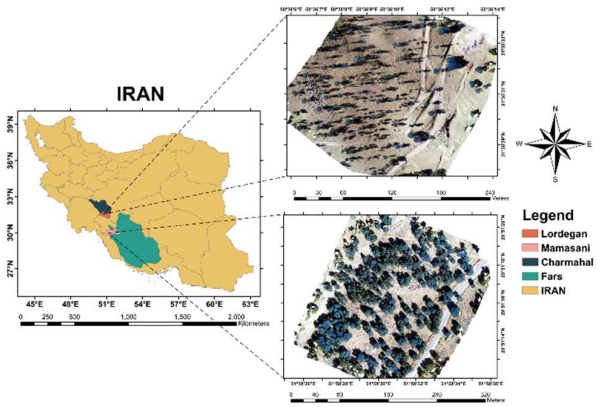

Figure 1. Study Areas shown on ortho mosaics of UAV-RGB imagery

The Fars site spans approximately 6.3 hectares at an average elevation of 2,290 m (Standard Deviation (STD): 6.9 m), while the Chaharmahal site covers about 3.6 hectares at 1,607 m (STD: 16.4 m) and lies along a souterrain slope. Dominant tree species across both sites is Brant´s oak (*Quercus brantii* Lindl.), typical of the region's semi-arid forests. The Fars site is characterized by a moderate level of decline, making it suitable for assessing early to mid-stage degradation. Conversely, the Chaharmahal site exhibited a generally high level of decline. The inclusion of these sites with distinct elevation, stand age structure, and degradation severity (Shafeian et al., 2025) was intended to enhance the robustness and generalizability of the approach.
In addition to climatic stressors, both sites are significantly affected by overgrazing via local livestock, which increases ecosystem pressure and impedes natural regeneration (Solaymani, 2015). These combined factors, along with the sites' accessibility and ecological representativeness, informed their selection for a remote sensing and machine learning-based forest decline analysis. A joint expert team from K. N. Toosi University of Technology and Iranian Research Institute of Forests and Rangelands conducted UAV flights using a DJI Phantom 4 Pro to capture high-resolution aerial imagery, enabling detailed visual assessments of tree health. To complement the remote sensing analysis, field reference data were collected through a systematic ground survey campaign.
On the ground, individual tree attributes were recorded, and decline severity was classified on a four-point ordinal scale (1 = low to 4 = severe). We applied the method proposed by (Ghasemi et al., 2024a) to convert these discrete severity classes into percentile estimates feasible for spatial extrapolation. This approach integrates UAV-derived RGB vegetation indices with field-based classifications to estimate tree-level decline severity. These estimates were then aggregated to the spatial resolution of Sentinel-2 imagery by computing the fractional tree cover and the weighted average decline severity within each pixel´s footprint.

2.2 Remote sensing data

Image processing of Sentinel-2 imagery was entirely conducted within the Google Earth Engine (GEE) platform, which provides access to both Level-2 harmonized products: Top-of-Atmosphere

(TOA) reflectance and Surface Reflectance (SR). While the SR product is available since March 28, 2017, the TOA archive extends back to June 27, 2015. The TOA imagery was used throughout this study to ensure temporal consistency and maximize historical depth.

A nine-year image time series (2016–2024) was compiled by selecting annual images within a fixed seasonal window from November 1st to November 14th, which was chosen to minimize phenological variability across years. Cloud-contaminated pixels were excluded using the Scene Classification Layer (SCL), and a median composite was generated for each year to produce stable, cloud-free representations of the study area. Digital Elevation Model from NASADEM (NASA JPL, 2020) was also incorporated into the stacked dataset to supplement the spectral data. Vegetation dynamics were assessed using a suite of spectral indices across four categories:

1. Normalized Difference (ND) indices: examples were the Green Normalized Difference Vegetation Index (GNDVI), Green Optimized Soil Adjusted Vegetation Index (GOSAVI), Global Vegetation Moisture Index (GVMI), Normalized Burn Ratio (NBR), Normalized Difference Red-Edge (NDRE), Normalized Difference Salinity Index (NDSI), Normalized Difference Vegetation Index (NDVI), Nonlinear Vegetation Index (NLI), Transformed Vegetation Index (TVI), and Weighted Difference Vegetation Index (WDVI), which were calculated to assess vegetation health across the visible, near-infrared (NIR), and shortwave-infrared (SWIR) bands. Indices such as GOSAVI and GVMI incorporate soil-adjusted terms to enhance sensitivity to biophysical variables (Ceccato et al., 2002).

2. Simple Ratio (SR) indices, including the Chlorophyll RedEdge (735/710) (CIRE), Chlorophyll Index RedEdge (CIred-edge), Green Difference Vegetation Index (GDVI), Green Ratio Vegetation Index (GRVI), Moisture Stress Index (MSI), Simple Ratio (800/500) (SI) and Simple Ratio (800/680) (SR), which primarily utilized red-edge and NIR bands to improve sensitivity to canopy structure and vegetation decline.

3. Complex vegetation indices such as the Enhanced Vegetation Index (EVI), Moderate Red-Edge Vegetation Index (MREVI), Soil Adjusted Vegetation Index (SAVI), Global Environment Monitoring Index (GEMI), Optimized Soil Adjusted Vegetation Index (OSAVI), Visible Atmospherically Resistant Index 700 (VATI) and Normalized Difference Moisture Index 2 (NDMI2) accounted for atmospheric noise and soil background effects through the use of correction coefficients and advanced formulations.

A multi-stage feature selection (FS) was employed to identify optimal predictors for two target variables: (1) the continuous Phenotypic Decline Index (PDI) derived from UAV-based assessments at the plot level (Ghasemi et al., 2022) and (2) the categorical decline into four discrete decline classes based on field observations. The workflow is shown in Figure **2**.

For the PDI, feature selection included three sequential steps. First, each feature was correlated with the PDI. Then, RF Feature Importance (RFFI) was applied to assess the explanatory power of individual features. Finally, Recursive Feature Elimination (RFE) was implemented to identify the most parsimonious subset of five predictive features. This approach was applied independently for each study site and vegetation index category to reduce redundancy and ensure optimal model performance (Demarchi et al., 2020).

A custom feature scoring approach was used for the classified decline dataset. Given the distinct characteristics between non-declined and declined samples, we plotted the 4 declined class centroids in the feature space and computed the distance vectors between them. The Δx for each two class was used as an indicator of discriminative power. Features were then ranked based on the average Δx across all class pairs, and those with positive Z_scores (Z_Score (Δx) > 0) were retained as relevant for classification purposes.

In the feature extraction (FE) stage, the objective was to preserve the original features while reducing multicollinearity and enhancing model interpretability. A Pearson correlation matrix was computed for the selected features, where highly correlated pairs ($|r| \geq 0.9$) were grouped. Partial Least Squares Regression (PLSR) (Wold et al., 2001) was then used to derive composite features from each group, capturing the shared variance. This dimensionality reduction was applied across all spectral index categories to ensure a compact and robust final feature set.

This hybrid framework enabled the development of predictive models that are both statistically robust and ecologically interpretable.

2.3 Machine Learning Model

Two RF configurations were used to model oak decline. For the classified decline dataset, a repeated 10-fold cross-validation (CV) on RF model was implemented using the ranger library (Wright and Ziegler, 2015). Class imbalance was addressed by applying class-specific weights and upsampling during training. The model was trained on 2019 data using multiclass performance metrics and a grid search over five tuning parameters. For the PDI, a regression-based RF model was constructed with an 80/20 train-test split.

Figure 2. Workflow of Feature Selection(FS) for both classified, and PDI data, along with Feature Extraction(FE).

2.4 Evaluation and trend generation

To evaluate model performance, both classification and regression outcomes were validated. For the classified data, predictions were assessed based on class probability distributions, prediction confidence, and year-wise class balance, providing insight into model reliability across different temporal inputs. In the regression case, model performance was evaluated using RMSE and R-squared statistics on holdout test data. Additionally, field surveys conducted between 2017 and 2021 in the Chaharmahal site provided a crucial reference for assessing tree health status, offering an independent benchmark to support predicted trends by the models.

The LOESS trend analysis was used to assess temporal decline patterns. Violin plots showed distribution of the predicted PDI. For classification, the dataset included 81 samples from Chaharmahal, 18 healthy samples from Fars, and 8 Class 1 declined samples, ensuring balanced representation across class variations. Due to lack of class 1 data in Chaharmahal, Classes 2 and 4 were excluded, focusing trends on Classes 1 and 3.

2.5 Climatic drivers of tree decline

We used Famine Land Data Assimilation System (FLDAS) FLDAS (McNally et al., 2022) data (1983–2025, 11132 m spatial resolution) on evapotranspiration, rainfall, soil moisture and soil temperature to analyze climatic drivers of oak decline. Monthly averages were extracted using GEE over the study areas. A sMK test was applied to detect directional trends over time, with Z-statistics plotted to visualize forward and backward trends for each variable.

3. RESULT AND DISCUSSION

3.1 Feature Engineering

PDI-based feature engineering was applied to each dataset individually as well as to their merged dataset. Figure 3 shows the correlation matrices for Chaharmahal, Fars and the merged dataset, both with and without feature engineering. In Fars, with generally healthier trees, correlations among indices were more distinct, while in Chaharmahal the pattern was affected by higher decline and mixed pixels. After feature engineering, 11 features were used for Chaharmahal, 10 for Fars, and 8 for the merged case, which showed the best R^2 and RMSE.

For categorical decline, a similar pattern was observed in the merged dataset (Figure 4). Here, the hybrid feature engineering algorithm selected 9 final features for classification, which were distinct from those selected for regression (e.g. only elevation and PLSR_RE overlapped with the original PDI features). This highlights the necessity of applying feature engineering to improve model performance.

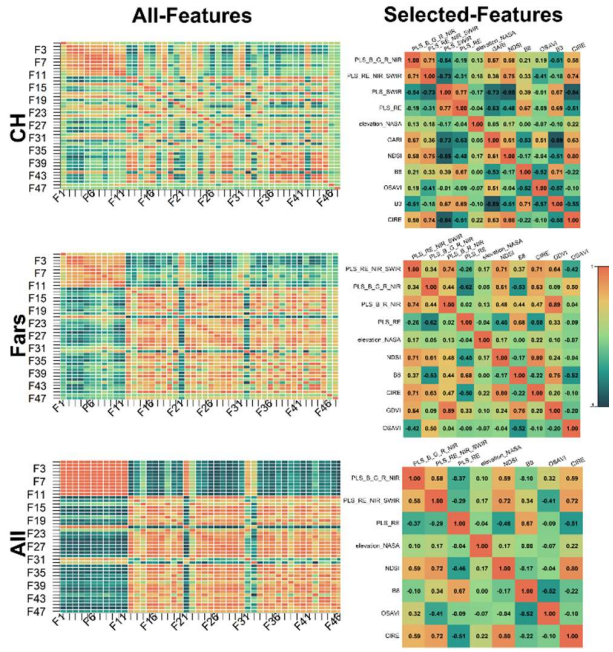

Figure 3. Correlation matrices of the PDI-based decline calculator for Chaharmahal (row 1), Fars (row 2), and the combined dataset (row 3). Results are shown for two scenarios: (1) using all available features and (2) using selected features derived through the proposed feature engineering method.

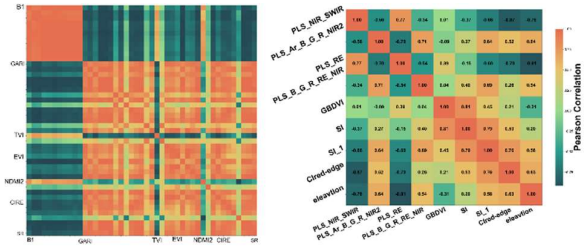

(A) (B)

Figure 4. Correlation matrices of the Classified-based decline with (A) all available features, and (B) using selected features derived via the proposed feature engineering method.

3.2 Decline predictor model

The PDI model using the merged dataset with feature engineering achieved the best performance, with an R^2 of approximately 0.6 and an relative RMSE of around 0.1 (Table 1). Results suggested that the feature selection applied to the combined data outperformed all other scenarios.

	CH	CH-FE	F	F-FE	All	All-FE
R^2	40	23	20	23	40	60
RMSE	0.13	0.13	0.14	0.14	0.13	0.10

Table 1. Model performance for Chaharmahal(CH) dataset, Fars(F), and merged version (All), with (FE). And without feature engineering.

Moreover, Table 2 summarizes the evaluation of the selected scenario for the classified decline data. A high F1 score of 0.87 for the 'No Decline' class indicated strong separability of this category. In contrast, the F1 score for class X0 was lower, at approximately 0.48, likely due to fewer samples and lower separability. Additionally, the model was unable to distinguish class X4, primarily because of the extremely limited number of the available samples.

Class	Precision	Recall	F1	Support
X0	0.830	0.907	0.867	54
X1	0.737	0.359	0.483	39
X2	0.556	0.750	0.638	60
X3	0.578	0.619	0.598	42
X4	0	0	NA	12

Table 2. Accuracy assessment of the classified decline using per-class performance metrics.

3.3 Trend generation

3.3.1 Decline:

The classified decline exhibited the trend shown in Figure **5** for class X1 (low decline) and class X3 (high decline). We observed that the number of high-decline trees rose significantly along with decrease in the number of low-decline trees. This pattern highlights an increasing trend of forest decline in both sites.

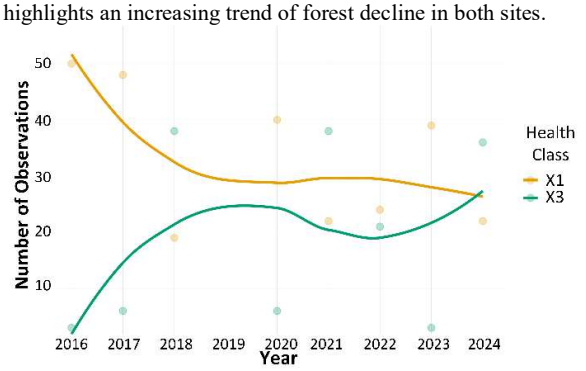

Figure 5. Decline trend from 2016 to 2024 based on class-wise data, focusing on low decline (Class X1) and high decline (Class X3).

Under the PDI scenario, the decline trend for the Fars site showed a noticeable decrease in the early years, followed by a relatively stable pattern after 2020 (Figure **6**). In contrast, the Chaharmahal site exhibited a more dynamic trend: an initial increase in decline, a period of stability, and a subsequent decrease toward 2024. Furthermore, fluctuations in both regions were significantly less pronounced compared to those observed in the classified scenario, indicating a rather moderate pattern of decline when assessed using the PDI approach. Notably, in the Chaharmahal data for 2020, an unexpectedly low decline value was observed compared to both the preceding and following years, an anomaly that might be attributed to external factors such as local variations in rainfall, human intervention (e.g. by partial removal of declined trees) or phenological shifts influenced by climatic variables in the specific year.

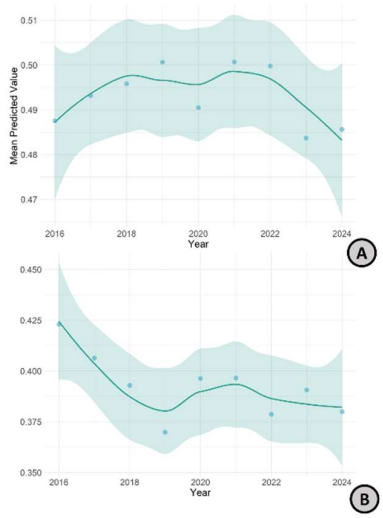

Figure 6. PDI-based decline trends from 2016 to 2024: (A) and (B) present LOESS-smoothed trends for Chaharmahal, and Fars sites respectively.

3.3.2 Climate

When analyzing the climatic data trends for both sites, the mean values were used to assess overall patterns in a longer timespan spanning beyond the period of remote sensing analysis. A significant decline in evapotranspiration began around 1996, with the trend stabilizing and becoming more consistent by approximately 2009. Rainfall trends showed a slight decrease starting around 2000, followed by a relatively stable pattern after 2020. While such fluctuations are inherent to climatic time-series data, vegetation may adapt to these changes over time through physiological or ecological resilience mechanisms.

The most pronounced decline was observed in soil moisture, showing a sustained drying trend across both sites during the analysis period. This trend exhibited high temporal consistency, supporting its use as a key variable in spectral trend derivation. Soil temperature variations were also examined, though these showed less statistical confidence ($p > 0.05$) in their trend significance during the study's timeframe. Further observation and data analysis are required to determine whether this trend is statistically significant.

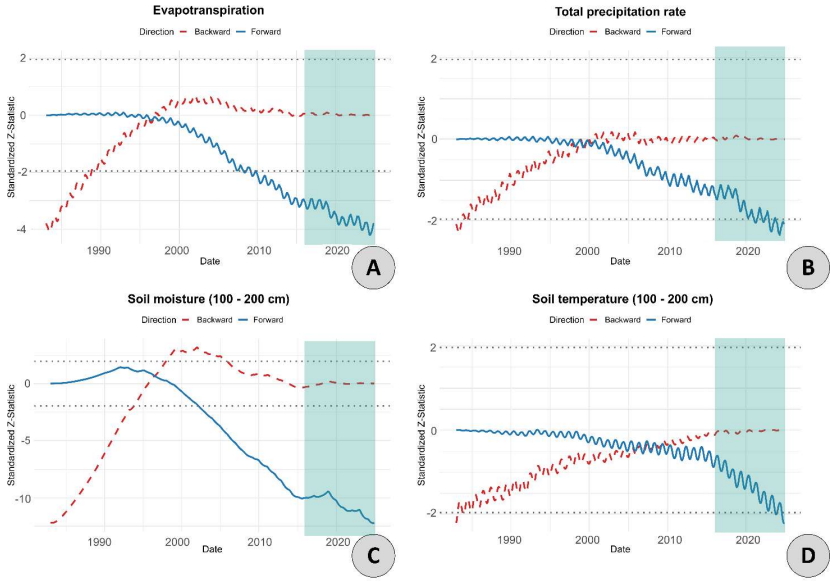

Figure 7. Trends in climatic variables from 1980 to 2025, analyzed using the sMK test: (A) Evapotranspiration, (B) Precipitation, (C) Soil Moisture, and (D) Soil Temperature. The study timespan was highlighted with a green shadow.

3.4 Trend analysis

Field observations conducted over a four-year period (2018 to 2021) provided detailed insights into tree decline across the Chaharmahal site. The observed trends (**Error! Reference source not found.**) wereFigure **9** categorized into five classes. Between 2018 and 2019, a noticeable increase in tree decline was recorded, characterized by a reduction in healthy trees and a sharp rise in the number of trees classified under Class 2 decline. The increase was still evident, although the overall trend remained relatively moderate and mostly stable in subsequent years. A similar pattern was also reflected in the PDI-based trend, with the exception of the year 2020 that showed some deviation from the mentioned pattern.

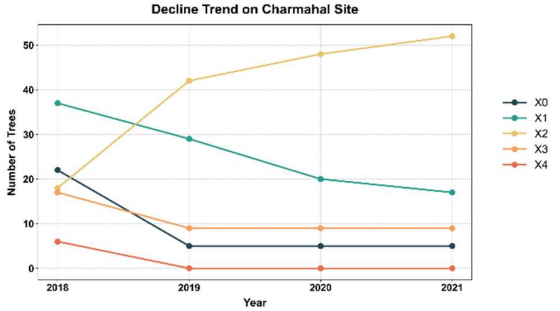

Figure 8. Observed decline trend based on annual in-situ field surveys.

Additionally, a decreasing trend in tree decline was observed after 2022. This is clearly demonstrated by a comparison between the UAV orthophoto plots from 2019 and 2024. The 2024 imagery revealed visibly healthier tree canopies, suggesting a recovery in vegetation health condition. This assessment is reliable, as phenological effects were minimized, i.e. the images were captured within the same seasonal window, ensuring consistency in observation. These visual indicators align with unpublished field observations, and reinforce the findings of reduced decline, particularly when cross-referenced with field and PDI-based evaluations.

The violin plots of predicted PDIs for both sites (Figure **9**) revealed distinct distribution patterns in tree decline between the Fars (A) and Chaharmahal (B) sites across 2016–2024. Fars exhibited tighter IQRs, reflecting more consistent decline rates, though a gradual Q1–Q3 expansion after 2021 implied emerging variability, potentially linked to trees adaptation to decline, management practices via for example establishing small aquifers for water preservation at tree roots, or even partial removal of declined trees by locals. Moreover, in Chaharmahal, the interquartile ranges (IQRs) showed notable variability, with Q1 and Q3 diverging significantly in drought-sensitive years (e.g. 2018–2020), suggesting heightened vulnerability to climatic stressors. Outliers above Q3 in post-2020 data indicate severe localized decline. Additionaly, Fars site demonstrated sharper skewness, emphasizing its ecological sensitivity, and lower mixed pixels. These distributional nuances complement the mean trends, underscoring site-specific resilience thresholds.

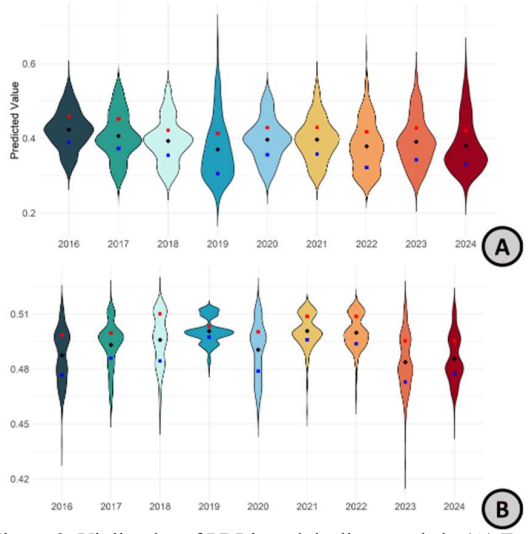

Figure 9. Violin plot of PDI-based decline trends in (A) Fars and (B) Chaharmahal sites.

All in all, this study demonstrated that remote sensing feature engineering coupled with trend analysis can notably improve decline prediction, with the merged dataset achieving optimal performance. The PDI-based model expectedly outperformed classification, yielding more consistent trends and underscoring its robustness for trend analysis. Decline patterns showed complex dynamics with limited alignment to climatic trends, which may indicate tree adaptation to environmental stressors. Field and UAV observations confirmed an increasing trend in decline during the early study period in Chaharmahal, followed by signs of recovery after 2022. The site located in the southern province of Fars displayed tighter decline distributions (possibly reflecting an unknown degree of resilience), i.e. less overall uncertainty. Together, these findings validate PDI's effectiveness while emphasizing the need to integrate ecological adaptation mechanisms into tree decline models. The results are to be still interpreted cautiously, but can extend the existing insights for a range of possible subsequent applications like developing early-warning systems of tree and forest decli8ne in ecologically-fragile and semi-arid areas like Zagros forests.

REFERENCES

Allen, C.D., Macalady, A.K., Chenchouni, H., Bachelet, D., McDowell, N., Vennetier, M., Kitzberger, T., Rigling, A., Breshears, D.D., Hogg, E.H. (Ted), Gonzalez, P., Fensham, R., Zhang, Z., Castro, J., Demidova, N., Lim, J.-H., Allard, G., Running, S.W., Semerci, A., Cobb, N., 2010. A global overview of drought and heat-induced tree mortality reveals emerging climate change risks for forests. Forest Ecology and Management 259, 660–684. https://doi.org/10.1016/j.foreco.2009.09.001

Breiman, L., 2001. Random Forests. Machine Learning 45, 5–32. https://doi.org/10.1023/A:1010933404324

Ceccato, P., Flasse, S., Grégoire, J.-M., 2002. Designing a spectral index to estimate vegetation water content from remote sensing data. Remote Sensing of Environment 82, 198–207. https://doi.org/10.1016/S0034-4257(02)00036-6

Choat, B., Jansen, S., Brodribb, T.J., Cochard, H., Delzon, S., Bhaskar, R., Bucci, S.J., Feild, T.S., Gleason, S.M., Hacke, U.G., Jacobsen, A.L., Lens, F., Maherali, H., Martínez-Vilalta, J., Mayr, S., Mencuccini, M., Mitchell, P.J., Nardini, A., Pittermann, J., Pratt, R.B., Sperry, J.S., Westoby, M., Wright, I.J., Zanne, A.E., 2012. Global convergence in the vulnerability of forests to drought. Nature 491, 752–755. https://doi.org/10.1038/nature11688

Cleveland, W.S., Devlin, S.J., 1988. Locally Weighted Regression: An Approach to Regression Analysis by Local Fitting. Journal of the American Statistical Association 83, 596–610. https://doi.org/10.1080/01621459.1988.10478639

De Jong, R., De Bruin, S., De Wit, A., Schaepman, M.E., Dent, D.L., 2011. Analysis of monotonic greening and browning trends from global NDVI time-series. Remote Sensing of Environment 115, 692–702. https://doi.org/10.1016/j.rse.2010.10.011

Demarchi, L., Kania, A., Ciężkowski, W., Piórkowski, H., Oświecimska-Piasko, Z., Chormański, J., 2020. Recursive Feature Elimination and Random Forest Classification of Natura 2000 Grasslands in Lowland River Valleys of Poland Based on Airborne Hyperspectral and LiDAR Data Fusion. Remote Sensing 12, 1842. https://doi.org/10.3390/rs12111842

Eliades, F., Sarris, D., Bachofer, F., Michaelides, S., Hadjimitsis, D., 2024. Understanding Tree Mortality Patterns: A Comprehensive Review of Remote Sensing and Meteorological Ground-Based Studies. Forests 15, 1357. https://doi.org/10.3390/f15081357

Fakhri, A., Latifi, H., 2021. A Consumer Grade UAV-Based Framework to Estimate Structural Attributes of Coppice and High Oak Forest Stands in Semi-Arid Regions. Remote Sensing 13, 4367. https://doi.org/10.3390/rs13214367

Fakhri, A., Latifi, H., Samani, K.M., Fassnacht, F.E., 2025. Introducing a computationally light approach to estimate forest height and fractional canopy cover from Sentinel-2 data. Journal of Arid Environments 228, 105343. https://doi.org/10.1016/j.jaridenv.2025.105343

Ghasemi, M., Latifi, H., Pourhashemi, M., 2024a. Integrating UAV and Freely Available Space-Borne Data to Describe Tree Decline Across Semi-arid Mountainous Forests. Environ Model Assess 29, 549–568. https://doi.org/10.1007/s10666-023-09911-3

Ghasemi, M., Latifi, H., Pourhashemi, M., 2022. A Novel Method for Detecting and Delineating Coppice Trees in UAV Images to Monitor Tree Decline. Remote Sensing 14, 5910. https://doi.org/10.3390/rs14235910

Ghasemi, M., Latifi ,Hooman, Shafeian ,Elham, Naghavi ,Hamed, and Pourhashemi, M., 2024b. A novel linear spectral unmixing-based method for tree decline monitoring by fusing UAV-RGB and optical space-borne data. International Journal of Remote Sensing 45, 1079–1109. https://doi.org/10.1080/01431161.2024.2305630

Hirschmugl, M., Gallaun, H., Dees, M., Datta, P., Deutscher, J., Koutsias, N., Schardt, M., 2017. Methods for Mapping Forest Disturbance and Degradation from Optical Earth Observation Data: a Review. Curr Forestry Rep 3, 32–45. https://doi.org/10.1007/s40725-017-0047-2

Immitzer, M., Neuwirth, M., Böck, S., Brenner, H., Vuolo, F., Atzberger, C., 2019. Optimal Input Features for Tree Species Classification in Central Europe Based on Multi-Temporal Sentinel-2 Data. Remote Sensing 11, 2599. https://doi.org/10.3390/rs11222599

Kirsch, M., Wernicke, J., Datta, P., Preisach, C., 2025. Early Detection of Forest Calamities in Homogeneous Stands -- Deep Learning Applied to Bark-Beetle Outbreaks. https://doi.org/10.48550/ARXIV.2503.12883

McNally, A., Jacob, J., Arsenault, K., Slinski, K., Sarmiento, D.P., Hoell, A., Pervez, S., Rowland, J., Budde, M., Kumar, S., Peters-Lidard, C., Verdin, J.P., 2022. A Central Asia hydrologic monitoring dataset for food and water security applications in Afghanistan. Earth System Science Data 14, 3115–3135. https://doi.org/10.5194/essd-14-3115-2022

NASA JPL, 2020. NASADEM Merged DEM Global 1 arc second V001. https://doi.org/10.5067/MEASURES/NASADEM/NASADEM_HGT.001

Pontius, J., Schaberg, P., Hanavan, R., 2020. Remote Sensing for Early, Detailed, and Accurate Detection of Forest Disturbance and Decline for Protection of Biodiversity, in: Cavender-Bares, J., Gamon, J.A., Townsend, P.A. (Eds.), Remote Sensing of Plant Biodiversity. Springer International Publishing, Cham, pp. 121–154. https://doi.org/10.1007/978-3-030-33157-3_6

Senf, C., Seidl, R., 2021. Persistent impacts of the 2018 drought on forest disturbance regimes in Europe. Biogeosciences 18, 5223–5230. https://doi.org/10.5194/bg-18-5223-2021

Shadmani, M., Marofi, S., Roknian, M., 2012. Trend Analysis in Reference Evapotranspiration Using Mann-Kendall and Spearman's Rho Tests in Arid Regions of Iran. Water Resour Manage 26, 211–224. https://doi.org/10.1007/s11269-011-9913-z

Shafeian, E., Ewald, M., Latifi, H., Fassnacht, F.E., 2025. Unveiling the main drivers of tree decline in Zagros semi-arid forests. Forestry: An International Journal of Forest Research 98, 410–425. https://doi.org/10.1093/forestry/cpae048

Simarmata, N., Wikantika, K., Tarigan, T.A., Aldyansyah, M., Tohir, R.K., Fauzi, A.I., Fauzia, A.R., 2025. Comparison of random forest, gradient tree boosting, and classification and regression trees for mangrove cover change monitoring using Landsat imagery. The Egyptian Journal of Remote Sensing and Space Sciences 28, 138–150. https://doi.org/10.1016/j.ejrs.2025.02.002

Solaymani, H., 2015. Impacts and Vulnerabilities of Climate change and SocioEconomic Challenges on Oak Forest Deterioration – west of Iran.

Torres, P., Rodes-Blanco, M., Viana-Soto, A., Nieto, H., García, M., 2021. The Role of Remote Sensing for the Assessment and Monitoring of Forest Health: A Systematic Evidence Synthesis. Forests 12, 1134. https://doi.org/10.3390/f12081134

Verbesselt, J., Hyndman, R., Newnham, G., Culvenor, D., 2010. Detecting trend and seasonal changes in satellite image time series. Remote Sensing of Environment 114, 106–115. https://doi.org/10.1016/j.rse.2009.08.014

Vicente-Serrano, S.M., Beguería, S., López-Moreno, J.I., 2010. A Multiscalar Drought Index Sensitive to Global Warming: The Standardized Precipitation Evapotranspiration Index. Journal of Climate 23, 1696–1718. https://doi.org/10.1175/2009JCLI2909.1

Wold, S., Sjöström, M., Eriksson, L., 2001. PLS-regression: a basic tool of chemometrics. Chemometrics and Intelligent Laboratory Systems, PLS Methods 58, 109–130. https://doi.org/10.1016/S0169-7439(01)00155-1

Wright, M., Ziegler, A., 2015. ranger: A Fast Implementation of Random Forests for High Dimensional Data in C++ and R. Journal of Statistical Software 77. https://doi.org/10.18637/jss.v077.i01